Article:
Clayton Da Silva, A., Akbar, T.F., Paterson, T.E. et al. (3 more authors) (2022) Electrically controlled click-chemistry for assembly of bioactive hydrogels on diverse micro- and flexible electrodes. Macromolecular Rapid Communications, 43 (23). 2200557. ISSN 1022-1336

https://doi.org/10.1002/marc.202200557

RESEARCH ARTICLE

Macromolecular Rapid Communications
www.mrc-journal.de

Electrically Controlled Click-Chemistry for Assembly of Bioactive Hydrogels on Diverse Micro- and Flexible Electrodes

*Aruã Clayton Da Silva, Teuku Fawzul Akbar, Thomas Edward Paterson, Carsten Werner, Christoph Tondera, and Ivan Rusev Minev**

The seamless integration of electronics with living matter requires advanced materials with programmable biological and engineering properties. Here electrochemical methods to assemble semi-synthetic hydrogels directly on electronically conductive surfaces are explored. Hydrogels consisting of poly (ethylene glycol) (PEG) and heparin building blocks are polymerized by spatially controlling the click reaction between their thiol and maleimide moieties. The gels are grown as conformal coatings or 2D patterns on ITO, gold, and PtIr. This study demonstrates that such coatings significantly influence the electrochemical properties of the metal-electrolyte interface, likely due to space charge effects in the gels. Further a promising route toward engineering and electrically addressable extracellular matrices by printing arrays of gels with binary cell adhesiveness on flexible conductive surfaces is highlighted.

1. Introduction

Based on natural or synthetic polymers, hydrogels can be engineered to mimic key functions of the extracellular matrix such as presentation of cell adhesion cues, sequestration and release of signalling molecules.[1,2] With their soft mechanical properties and high water content (>90%), they can act as malleable scaffolds to allow infiltration of cells in tissue-engineered systems.[3] Recently, hydrogels have shown promise as materials for bridging the gap between living matter and electronics.[4,5] Thus, much effort is concentrated on developing hydrogels as coatings on electronic materials.[6,7] Applications range from implantable electrode arrays to organoid cell culture. For example, due to elastic moduli in the range of kilopascals, they can be used to address the mechanical mismatch between metallic electrode surfaces and brain tissue.[8] Further, their biochemical properties can be harnessed to control the interaction with cells of the host tissue.[9] However, strategies for forming hydrogels on or around conductive surfaces are still few and complex, for example, requiring silanization of the interacting surface. Most gelation strategies require either a mold into which the reaction can proceed under spatial confinement or complex inkjet printing strategies where the pre-gel components are combined in situ.[10,11] This makes the creation of conformal coatings on arbitrary conductive, 3D surfaces challenging. Furthermore, most hydrogel polymerization methods exploit radical polymerization initiators, for example, thermal-, photo- or chemical initiators.[12,13] Electrochemical methods where water hydrolysis and the associated localized pH changes are used to form gels on electrodes have also been explored. A number of systems based on chitosan,[14,15] alginic acid,[16] alginate with calcium carbonate,[17] collagen[18,19] and silk[20,21] have been demonstrated. However, these mainly result from precipitation and modifying weak interactions between macromolecules, rather than the formation of covalent bonds. Other electrochemical methods for gelation have also been employed but require redox mediators such as ferrocene dimethanol, acetosyringone, or potassium hexachloroiridate(III).[22] Apart from the fact that the biocompatibility of these methods may not be sufficient, control over the reaction itself is limited, making it complicated to create coatings with defined physical and biochemical properties.

Here we demonstrate an electrochemically controlled method for crosslinking glycosaminoglycan (GAG) containing hydrogels on various conductive surfaces. We use a versatile system of PEG-heparin hydrogels that can be polymerized via

A. C. Da Silva, T. E. Paterson, C. Tondera, I. R. Minev
Department of Automatic Control and Systems Engineering
Faculty of Engineering
University of Sheffield
Mappin Street, SheffieldS1 3JD, UK
E-mail: i.minev@sheffield.ac.uk
A. C. Da Silva, I. R. Minev
Insigneo Institute for in silico Medicine
University of Sheffield
Pam Liversidge Building, SheffieldS1 3JD, UK
T. F. Akbar, C. Werner, C. Tondera, I. R. Minev
Institute of Biofunctional Polymer Materials
Leibniz Institute of Polymer Research Dresden
Hohe Str. 6, 01069 Dresden, Saxony, Germany

The ORCID identification number(s) for the author(s) of this article can be found under https://doi.org/10.1002/marc.202200557

DOI: 10.1002/marc.202200557

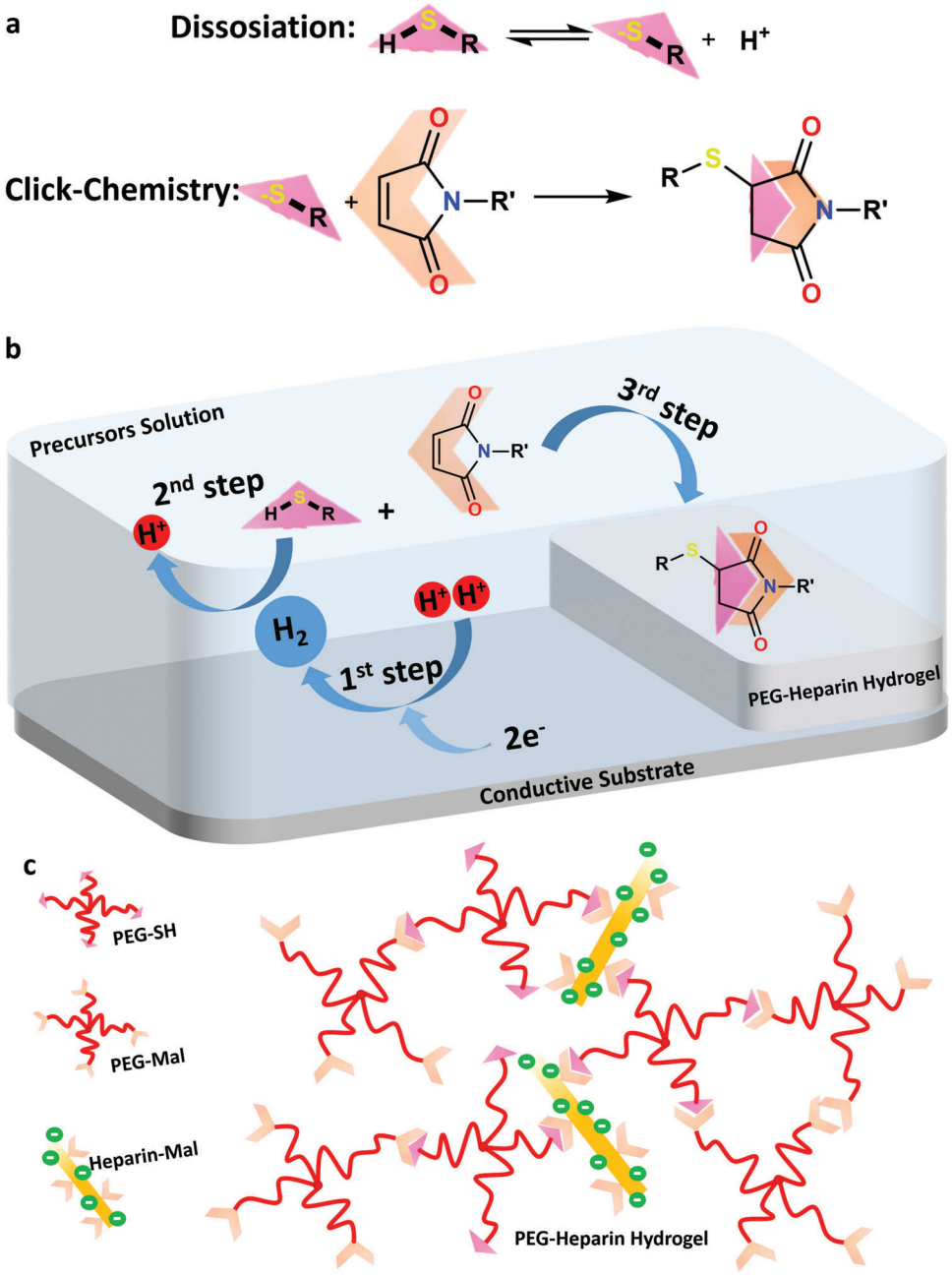

Figure 1. Direct electro-assisted PEG-heparin hydrogel formation. a) Chemical reaction of the thiol (purple) dissociation to thiolate followed by click chemistry conjugation of the thiolate and maleimide (orange) functional groups. b) Schematic representation of the general ECC mechanism here adapted to the specifics of PEG-heparin hydrogel deposition. In acidic media, protons (red spheres) are reduced over the electrode (receiving electrons), forming hydrogen gas (blue sphere). The electrochemical reaction reduces the concentration of protons locally at the interface (functioning as a base), thereby facilitating the dissociation of thiol groups and triggering the polymerization reaction of PEG-heparin hydrogel. In our system, *R* is four-arm PEG and *R′* is either four-arm PEG or heparin. c) Schematic representation of the PEG-heparin hydrogel biomatrix. Due to the polyanionic nature of heparin, the biomatrix is fully negatively charged and highly hydrophilic. The role of the PEG-Mal component here is to ensure that the cross-link density of the gel remains the same when the concentration of the Heparin-Mal component is changed (or altogether removed).[23]

biocompatible thiol-maleimide click chemistry reactions (Michael-type addition) without intermediaries or byproducts. These hydrogel systems have shown promise as versatile semi-synthetic materials for controlling cell-matrix interactions but have not yet been integrated into conducive materials.[11,23] By indirectly controlling the click chemistry reaction, we assembled well-defined covalent cross-linked gels on gold, platinum-iridum (PtIr), indium tin oxide (ITO) flat surfaces and freestanding structures such as electrode tips. Apart from creating conformal coatings, we demonstrate the patterning of hydrogel dot arrays

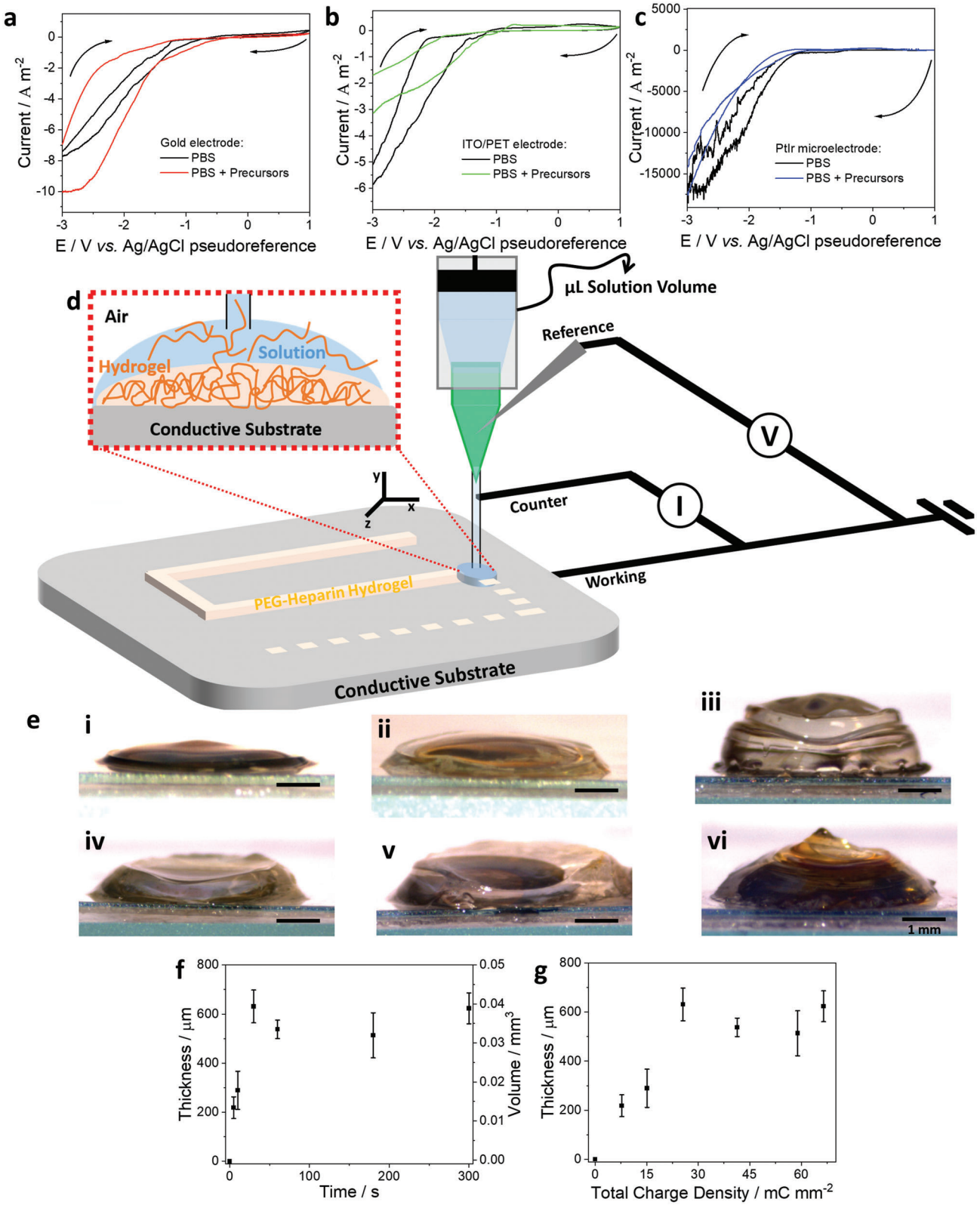

Figure 2. Electrochemistry and growth profiles for PEG-heparin hydrogel. a–c) Cyclic voltammetry of gold electrode (red), ITO/PET (green) and PtIr microelectrode (blue), respectively, using 0.01× PBS as supporting electrolyte (black), a scan rate of 100 mV s^{-1}. d) Schematic of the 3-electrodes system adapted using customized printing nozzle with integrated pseudo reference electrode enabling electrochemistry experiments in microliter volume (≈100 µL). e) Representative microscope images (side view) of the growth profile of PEG-heparin hydrogel for i) 5, ii) 10, iii) 30, iv) 60, v) 180, and

with binary cell adhesiveness on a flexible conductive surface. Our approach addresses a critical bottleneck in integrating bioactive materials with electronic conductors.

In our model gel system, a click chemistry reaction between thiol groups and maleimide enables step-growth polymerization of gels consisting of PEG and heparin building blocks.[23–25] In acidic media, the thiol group is protonated, which inhibits the reaction with maleimide. When the pH of the solution is increased, the gelation reaction is enabled, leading to the formation of a bulk gel taking the shape of the reagent container. The approach presented here is different because it establishes local control of pH in the vicinity of the electrode surface, enabling spatial control over the click reaction. Water hydrolysis occurs at the electrode–electrolyte interface under a suitable electric potential (lower than −1.5 V versus Ag/AgCl pseudoreference). In an acidic electrolyte, the semi-reaction at the cathode is 2 protons receiving 2 electrons obtaining hydrogen gas.[26] This reaction promotes the depletion of protons close to the electrode interface. When thiol groups are present in the solution, it triggers the dissociation step creating reactive thiolate groups (**Figure 1**a). This is followed by a reaction with maleimide groups and the formation of a covalent PEG-heparin hydrogel (Figure 1b,c). The general mechanism follows an electrochemical–chemical–chemical (ECC) transformation.

2. Results and Discussion

Water hydrolysis can be triggered on electrode surfaces made from a variety of materials. **Figure 2**a–c shows cyclic voltammetry profiles of gold, ITO, and PtIr alloy electrodes in PBS. It is possible to see within the electrochemical windows of −3.0 to +1.0 V that the water hydrolysis starts at around −1.5 V, accompanied by hydrogen gas generation (Figure S1, Supporting Information). The addition of the hydrogel precursors to the electrolyte does not result in significant changes or the appearance of new electrochemical peaks. This suggests that there is no direct electron transfer between the gel precursors and the electrodes, meaning that the precursors do not directly participate in electrochemical reactions. We conducted our gelation experiments in small liquid droplets (10 µL) placed on large flat conductive surfaces. This allows us to work with minute quantities of reagents and defines the spatial extent of the gel. As illustrated in Figure 2d, potentiostatic control of the reaction is enabled by introducing a counter and reference electrode in contact with the liquid droplet. PEG-heparin gels can be formed in only several seconds by triggering the water hydrolysis reaction. Figure 2e shows representative microscope images of hydrogel growth using i) 5, ii) 10, iii) 30, iv) 60, v) 180 and vi) 300 s, respectively, under −3.0 V (versus Ag/AgCl pseudoreference) on ITO/PET substrates. The corresponding chronoamperometry profiles of the electrodeposition are shown in Figure S2, Supporting Information. The gels initially exhibit a linear growth profile, followed by a plateau (Figure 2f). We hypothesize that when the hydrogel reaches ≈600 µm thickness (0.04 mm^3), the diffusion of protons from the conductive surface through the already formed gel is significantly hindered, leading to a reduced reaction rate. This is supported by the observation that electropolymerization currents drop significantly when the plateau is reached, evidencing a lower reaction rate (Figure S2e,f, Supporting Information). Figure 2g illustrates that the growth of the gel is controlled by the amount of charge supplied. The linear correlation between total charge density and the thickness/volume (up until the saturation point at ≈25 mC mm^{-2}) demonstrates that all electrons consumed at the electrode interface have generated hydrogel, in agreement with the ECC mechanism proposed above (Figure 1b). Changing the initial rate of the reaction by more negative electrode potentials (faster rate of proton generation) was not observed to influence the plateau thickness of gels (Figure S3, Supporting Information). In polymerized gels we did not observe trapped gas bubbles, likely because electrochemically generated hydrogen gas dissolves and diffuses away from the gel–electrode interface.

We next attempted to polymerize PEG-heparin gel on a microelectrode formed from the de-insulated tip of a Polyimide coated PtIr microwire (**Figure 3**a). In this setup, the tip of the wire (100 µm) acts as the WE and is placed inside the PBS droplet (20 µL) containing gel precursors. The droplet is resting on a gold surface, which acts as the CE (area defined by the droplet footprint), and an additional microwire (Ag/AgCl) is inserted as RE. Figure 3b shows representative optical microscope images of the PEG-heparin hydrogel grown on the microelectrode (WE) using i) 0.1, ii) 0.2, iii) 0.5, iv) 1, v) 2 and vi) 5 s, respectively, under −3.0 V (versus Ag/AgCl pseudoreference). Representative electrodeposition profiles are shown in Figure S4, Supporting Information. In this geometry, diffusion of electrochemically generated protons is radial and results in the formation of a sphere of gel growing from the microelectrode tip.[27–29] We observe a linear growth of the radius of the sphere with time and total charge density (Figure 3c,d). An inflection point at 1 s (−3.3 mC mm^{-2}) indicates a decrease in the growth rate from 695 ± 89 (−2015 ± 75 mm^3 mC^{-1}) to 399 ± 50 µm s^{-1} (−902 ± 20 mm^3 mC^{-1}). The decrease in the growth kinetics is associated with a plateau in the current after the inflection point (Figure S4, Supporting Information). Different from gelation in the planar geometry, where the growth reached a plateau, radial diffusion (coming from all directions) significantly increases mass transport to the electrode interface for the microelectrode. Although the growth rate kinetics decreases, the presence of the hydrogel does not completely block the diffusion of ions, and the hydrogel continues to grow.[30]

To investigate how the PEG-heparin coating affects the electrochemical properties of the electrode tip, we performed cyclic voltammetry and impedance spectroscopy measurements (Figure 3e,f). On bare PtIr in PBS, we observe proton absorption at potentials more negative than −0.5 V (versus Ag/AgCl pseudoreference) and the absence of Faradaic peaks in the anodic (positive potential) region.[31] In contrast, on PtIr, coated with PEG-heparin hydrogel, Faradaic (red-ox) peaks typical of platinum emerge.[32,33] In impedance spectra, higher values for the

vi) 300 s, respectively, under −3.0 V (versus Ag/AgCl pseudoreference) on ITO/PET substrates. f) Thickness growth of PEG-heparin hydrogel as a function of polymerization time. g) Relationship between thickness and total charge density supplied to promote the gelation reaction of the PEG-heparin hydrogel. Here, thickness and volume are measured quantities with the error bars representing the mean ± standard deviation (n = 3 independent electrodeposition experiments).

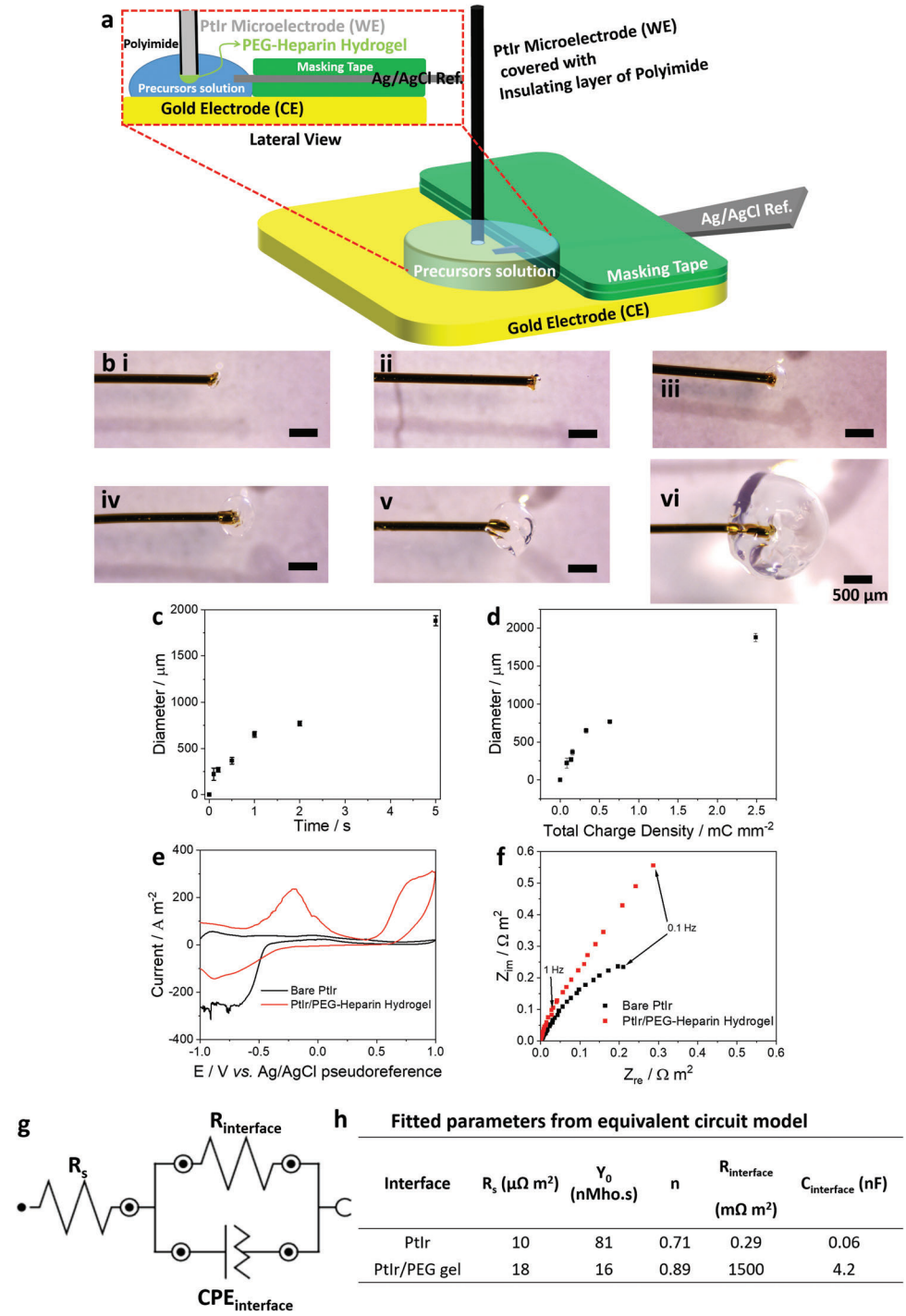

Interface	R_s (µΩ m²)	Y_0 (nMho.s)	n	$R_{interface}$ (mΩ m²)	$C_{interface}$ (nF)
PtIr	10	81	0.71	0.29	0.06
PtIr/PEG gel	18	16	0.89	1500	4.2

Figure 3. Electrodeposition of PEG-heparin hydrogel over PtIt microelectrode. a) Schematic representation of the electrochemical setup adapted to promote the electrodeposition on the tip of a PtIr microwire immersed in a droplet of precursors. Inset: lateral view of the setup. b) Representative optical microscope images of the growth profile of PEG-heparin hydrogel (spheroids) for i) 0.1, ii) 0.2, iii) 0.5, iv) 1, v) 2, and vi) 5 s, respectively, under −3.0 V (versus Ag/AgCl pseudoreference). c) Growth profile by diameter size of PEG-heparin hydrogel as a function of time. d) Growth profile by total charge density supplied to promote the gelation reaction. e) Cyclic voltammetry of bare PtIr (black) and gel coated (red) microwire tips in PBS as supporting electrolyte at scan rate of 100 mV s^{-1}. f) EIS showing Nyquist plot of bare PtIr (black) and gel coated (red) microwire tips. The PEG-heparin hydrogel is deposited in 5 s. g) Modified Randles equivalent circuit used to model the electrical properties of hydrogels, R_s indicates electrolyte resistance, $R_{interface}$ is the interface resistance and $CPE_{interface}$ is the constant phase element for the interface. h) Equivalent circuit parameters extracted from impedance spectra, where Y_0 is the admittance, n ($0 \leq n \leq 1$, unitless) is the deviation from ideal capacitive behavior and $C_{interface}$ is the capacitance at the interface.

imaginary part indicate a higher capacitance for electrodes coated with PEG-heparin gel (Figure 3e). By fitting a modified Randles circuit to impedance spectra, we obtain values for the putative electronic components describing the interface (Figure 3g and Figure S5, Supporting Information).

Resistance and capacitance increase from 0.29 to 1500 mΩ m^2 (≈5000 times) and 0.06 to 4.2 nF (≈70 times) for bare and coated PtIr, respectively. As the PEG-heparin hydrogel does not have any electronic conductivity, a large increase in resistance is expected once the insulating hydrogel covers the active electrode surface. The emergence of redox peaks and much-increased capacitance of coated electrodes may be linked to the distribution of stationary and mobile charges in the gel. Covalently cross-linked gels containing heparin (a highly sulfated GAG) have a high negative space charge at physiological pH.[10,23] Although heparin molecules are bound in the polymer matrix, their charges have to be compensated by mobile charged ions migrating from the electrolyte. This may cause enhanced charge separation close to the electrode surface. In other words, a higher concentration of mobile charges in the diffuse layer close to the metal electrode may lead to increased capacitance and more pronounced redox peaks.

Apart from assembling conformal coatings, our approach can enable the patterning of gels in 2D. Confining the gelation reaction within a droplet is a convenient way to limit the footprint of the gel (Figure 2a). By introducing lateral movement of the nozzle, it is possible to pattern arbitrary shapes of gel on continuously conductive surfaces. **Figure 4**a shows a line of PEG-heparin gel printed on a flexible ITO/PET substrate. During the printing process, the deposition current is stable (Figure 4a-ii). The red asterisk denotes an intentional gap in the line made by lifting the nozzle. It evidences that the solution closes the circuit and is necessary to sustain the gelation reaction. We used this discontinuous approach to pattern arrays of separated gel dots (Figure 4b). Individual gel dots show good adhesion to the substrate under compressive or tensile stress induced by bending (Figure 4b-i,ii) and following swelling in PBS, although swelling causes some islands to merge. The brown color observed in gels deposited on ITO is attributed to the generation of indium and tin nanoparticles generated by negative electric potential[34] (Figure S1b, Supporting Information). In contrast with more established electroassembly techniques,[35] our approach does not require a pre-patterned conducive layer (e.g., Gold) or the immersion of the whole structure in solution. Thus, by handling the electrochemical reaction in a droplet, small volumes of expensive reagents can be used and CAD generated designs in 2D can be rapidly realized by moving the nozzle. This comes at the expense of reduced lateral resolution which is determined by the nozzle size and liquid spreading on the conductive substrate. Optimization of the latter two parameters have resulted in demonstrations of electrodeposited patterns at sub-millimeter resolution.[36,37]

Finally, we demonstrate arrays where individual dots have different gel compositions (Figure 4c-i). Dots are made from PEG-heparin or gels that only contain PEG (PEG-PEG). The gel dot arrays were stable in PBS for at least 3 days and showed no dissolution or delamination from the substrate. We seed the arrays with the neuron-like cell line NG108. As illustrated in Figure 4c-ii–v, the presence or absence of heparin governs notable differences in the number and morphology of adherent cells. This is evidence that heparin retains its bioactivity following the electropolymerization process. While we do not claim a comprehensive characterization of the biomatrix, we hypothesize that heparin provides a favorable environment for cell adhesion by immobilizing matrix factors either secreted by the cells or available in the culture serum (fetal calf serum and L-glutamine).

Our approach demonstrates a promising route where electrochemical polymerization can be applied for coating electrodes with bioactive matrices. By electronically controlling the amount of generated charges, the reaction leading to hydrogel synthesis can be precisely controlled so that a specific amount of the biohybrid material (PEG-heparin hydrogel) can be synthesized on the electrode surface.[38] We used a hydrogel containing heparin, a highly sulfated GAG because it resembles the heparan sulfate of extracellular matrices. The native extracellular matrix is rich in GAGs which complex multiple soluble signalling proteins (cytokines and growth factors) and thereby modulate their spatiotemporal distribution, stability, and activity. In neural tissues, chondroitin sulfate and heparan sulfate polymers play important roles in maintaining synapse connections, the milieu of soluble factors, and can be remodelled in response to injury.[39] Improved tolerance and functionality of implanted electronics may therefore depend on our ability to integrate elements of the ECM with electronic conductors. Due to their high degree of sulfation and associated space charge, GAG hydrogels also appear to modify the electrochemistry of the metal–electrolyte interface, an important consideration for the design of neural probes. Our approach is potentially applicable to a wide range of thiol-ene chemistry reaction systems.[40] Good spatial and temporal control of the reaction combined with the covalent nature of the bond may open possibilities in other areas for example in biosensor functionalization.[41–44]

3. Conclusion

The work presented here adds one more mechanism to a growing list of electrochemical hydrogelation approaches. We present for the first time an electrochemically induced crosslinking method based on a biocompatible maleimide-thiol click chemistry reaction. By applying a defined potential, protons at the cathode are reduced, making the cathode operating as a proton acceptor. This leads to a locally defined increase in pH, which subsequently induces the thiol-maleimide click reaction. We demonstrate that this method can coat various electrode materials such as gold, ITO, and PtIr in arbitrary shapes such as planar sheets or microelectrodes. By combining the method with a commercially available 3D printing setup, defined hydrogel shapes and structures can also be printed. In perspective, our reported findings can pave the way for electronic tissue–device interface technologies employing the incorporation of conductive particles or conductive polymers within soft and bioactive hydrogel coatings.

4. Experimental Section

Materials: The hydrogel precursor solutions consisted of three polymers: thiol-conjugated four-arm polyethylene glycol (PEG-SH, Mr = ≈10 000 g mol^{-1}), maleimide-conjugated four-arm polyethylene glycol (PEG-mal, Mr = ≈10 000 g mol^{-1}), and maleimide-conjugated heparin

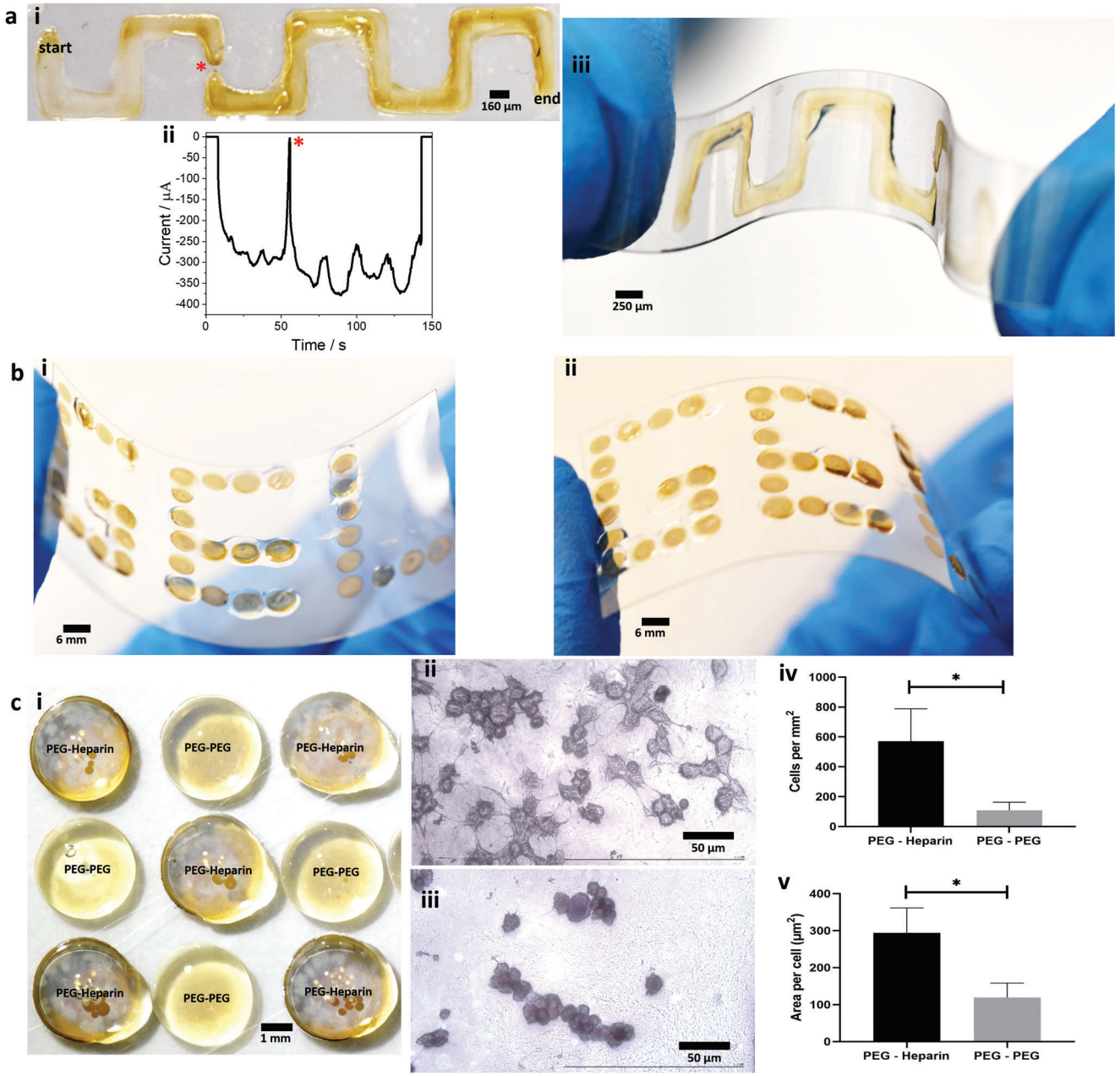

Figure 4. Electro-assisted PEG-heparin hydrogel printing/patterning. a) Line of PEG-heparin hydrogel with 90° turns on ITO/PET substrate (i). ii) Chronoamperogram along the printing experiment under −3.0 V (versus Ag/AgCl pseudoreference). Red asterisk denotes the intentional gap in the patterning. iii) The patterned PEG-heparin hydrogel under bending. b) Dot array with PEG-heparin hydrogel ($Q = -9.6 \pm 1.1$ mC for $n = 39$). Concave (i) and convex (ii) bending of the dot array. c) Picture of 3 × 3 dot array (i) with alternating pure PEG-PEG and PEG-heparin (corners and center) hydrogels. Microscope images of H&E stained NG108 cells cultured for 24 h on PEG-heparin (ii) and PEG-PEG gel dots (iii) revealing a greater number of cell/neurite extensions on PEG-heparin than PEG-PEG gels. Cell density (iv) and area per cells (v) on 3 × 3 PEG dots array hydrogel counted in a 1.0 mm^2 area. Three replicates of each gel type, two-tailed *t*-test to reject null hypothesis at $p < 0.05$, plotted on graph is mean ± standard deviation.

(Hep-mal, Mr = ≈15 000 g mol^{-1}). Both conjugated PEGs were obtained from JenKem Technology, USA, and Hep-mal was synthesized in-house.

Precursors Solution: Hep-mal, PEG-mal, and PEG-SH were dissolved in 0.01× PBS pH 2.14 (adjusted with 1 M HCl) before mixing to obtain final concentrations of 2.5×10^{-4} for Hep-mal, 1.4×10^{-3} M for PEG-mal, and 1.7×10^{-3} M for PEG-SH. This composition resulted in 3.4 wt% solid content and 11 µmol mL^{-1} ionizable sulfate groups per hydrogel volume in the swollen state. The ratio of the maleimide compared to the thiol groups was 1:1, resulting in a crosslinking degree of $\gamma = 1$. For PEG-PEG hydrogels, the concentrations of both PEG-mal and PEG-SH were 1.8 10^{-3} and 1.3 10^{-3} M, respectively.

Electrochemical Measurements In Situ: Cyclic voltammetry (CV), chronoamperometry (CA), and electrochemical impedance spectroscopy (EIS) were performed using a portable potentiostat (PalmSens4 controlled

using PSTrace 5.8 software) coupled to the 3D printer. Electrochemical impedance spectroscopies (EIS) were recorded from 1 MHz to 0.1 Hz, with excitation amplitude of 10 mV (RMS) at 10 points per decade. The working electrode was gold foil 0.10 mm thick, 2.0 × 2.0 cm^2 (Goodfellow, 99.95% purity), indium-tin oxide coated polyethylene terephthalate (ITO/PET, resistivity 60 Ω/sq, Sigma-Aldrich) cut in rectangular shape 4.0 × 1.0 (for the line patterning) and 8.0 × 5.0 cm^2 (for the GEL dotted patterning) or single strand microcable of PtIr microelectrode (100 µm of electrode area) coated with thin layer of PTFE (Sandivik). The counter electrode was the stainless steel dispensing needle (840 µm inner diameter, 1270 µm outer diameter, and 12.7 mm length) of a commercially available printing nozzle (Intertronics, FIS5601099) or the gold foil (for PtIr microelectrode experiments). The reference electrode was prepared using silver wire 0.10 mm diameter, 2 cm length (Goodfellow, 99.99% purity) covered with electrodeposited silver chloride (AgCl) according to published protocols.[45] Briefly, the silver wire electrode was immersed in potassium chloride 3 mol L^{-1} solution and the open circuit potential was measured for 300 s. Later, at + 50 mV above, the open circuit potential was applied for 1800 s. The reference electrodes were used in two different conditions. The first was fixed between two masking tapes for the PtIr microelectrode experiment. The second was inserted in the printing nozzle and secured in place by partially melting its plastic casing and further fixed with cyanoacrylate glue. The reference electrode was immersed in the precursor solution. However, it did not make electrical contact with the needle counter electrode. This assembly was herein referred to as a customized printing nozzle. Total charge density (C mm^{-2}) was calculated by $Q = I \times t$, where I is the current density (A mm^{-2}) and t is time (s). The modified Randles equivalent circuit model was applied to extract values for the constant phase element (CPE) and resistivity of hydrogels. Parameter fitting was conducted using the NOVA 2.1 software (Metrohm Autolab). Capacitance was calculated from the constant phase element (CPE) using $C_{\text{interface}} = \frac{\sqrt[n]{R_{\text{interface}} \times Y_0}}{R_{\text{interface}}}$, where $C_{\text{interface}}$ is the capacitance of the hydrogel (Farad), $R_{\text{interface}}$ is the resistance of the interface/hydrogel (Ω m^2), i_0 is the admittance (Mho or Siemens), and n is the deviation from ideal capacitive behavior.[46]

Electro-Assisted Printing Procedure: The customized printing nozzle was attached to a syringe containing precursors solution and mounted on the bioprinter 3D Discovery (RegenHU, Switzerland). The working electrode (WE) (ITO/PET) was laid flat on the printing platform, and a droplet of precursors solution was dispensed on the surface. The customized nozzle was brought above the plate in contact with the droplet. For printing of the line, precursors solution was continuously dispensed through the dispensing needle with a flow of 0.02 µL s^{-1}. The patterns of the curved line and the GEL dots were generated in G-code with the software BioCAD. Following deposition, hydrogels were gently rinsed with deionized water to remove any macromolecule, unpolymerized monomers or reaction byproducts, and stored in PBS solution. The thickness, area, and volume of the generated hydrogels were obtained from optical micrographs (Stemi 508 Compact Greenough Stereo Microscope, Zeiss) with ImageJ software using spherical segments from a top view and cylinder from a lateral view. All experiments were made in triplicate using freshly prepared solutions. Unless stated otherwise, data are reported as the mean ± standard deviation.

Neuronal Cell Culture: NG108-15 cells (ECACC 88 112 303) were cultured in DMEM (Sigma, UK) with 10% FBS (Biosera, UK), 1% L-glutamine (Sigma, UK), 1% penicillin-streptomycin (Sigma, UK), 0.2% Amphotericin B (Sigma, UK) and passaged as required. Alternating 3 × 3 grid gel samples were submersed in 3 mL of media in 12-well plates (ThermoFisher, UK), and 200 000 cells were added. Samples and cells were incubated for 24 h at 37 °C. Samples were rinsed and fixed for 10 min in 37% formaldehyde (Sigma, UK).

H&E Staining and Imaging: To image cells through an optical microscope, hematoxylin and eosin (H&E) staining was used to stain nuclei and cell bodies. Samples were submerged in hematoxylin for 90 s before being placed in running tap water for 5 min. The samples were then placed in eosin solution for 5 min before gentle washing with tap water. Dehydration of the sample was achieved by a 3 s submerging in 70% IMS, a 30 s submersion in 100% IMS, and a final 3 s submersion in xylene. After all solution evaporated, the samples were imaged on an optical microscope. Multiple images were combined into a single image by the File → Automate → Photomerge function in Adobe Photoshop (Adobe, USA). Cells were counted on ImageJ (1.2 mm^2) and adjusted to a 1 mm^2 area. *t*-test was used to test statistical significance ($n = 3$).

Supporting Information

Supporting Information is available from the Wiley Online Library or from the author.

Acknowledgements

A.C.D.S. and T.F.A. contributed equally as first authors. C.T. and I.R.M contributed equally in the supervision of the work. All authors acknowledge funding from ERC Starting Grant: IntegraBrain (804005).

Conflict of Interest

The authors declare no conflict of interest.

Data Availability Statement

The data that support the findings of this study are available from the corresponding author upon reasonable request.

Keywords

click chemistry, electrochemistry, glycosaminoglycans, hydrogels, microelectrodes

Received: June 30, 2022
Published online:

[1] C. Tondera, R. Wieduwild, E. Röder, C. Werner, Y. Zhang, J. Pietzsch, *Adv. Funct. Mater.* **2017**, *27*, 1605189.
[2] N. Lohmann, L. Schirmer, P. Atallah, E. Wandel, R. A. Ferrer, C. Werner, J. C. Simon, S. Franz, U. Freudenberg, *Sci. Transl. Med.* **2017**, *9*, 1.
[3] X. Li, B. Cho, R. Martin, M. Seu, C. Zhang, Z. Zhou, J. S. Choi, X. Jiang, L. Chen, G. Walia, J. Yan, M. Callanan, H. Liu, K. Colbert, J. Morrissette-Mcalmon, W. Grayson, S. Reddy, J. M. Sacks, H. Q. Mao, *Sci. Transl. Med.* **2019**, *11*, eaau6210.
[4] C. M. Tringides, N. Vachicouras, I. De Lázaro, H. Wang, A. Trouillet, B. R. Seo, A. Elosegui-Artola, F. Fallegger, Y. Shin, C. Casiraghi, K. Kostarelos, S. P. Lacour, D. J. Mooney, *Nat. Nanotechnol.* **2021**, *16*, 1019.
[5] H. Yuk, B. Lu, S. Lin, K. Qu, J. Xu, J. Luo, X. Zhao, *Nat. Commun.* **2020**, *11*, 1604.
[6] N. Rossetti, P. Luthra, J.'E. Hagler, A. H. J. Lee, C. Bodart, X. Li, G. Ducharme, F. Soavi, B. Amilhon, F. Cicoira, *ACS Appl. Bio Mater.* **2019**, *2*, 5154.
[7] J. Goding, A. Gilmour, P. Martens, L. Poole-Warren, R. Green, *Adv. Healthcare Mater.* **2017**, *6*, 1601177.
[8] S. P. Lacour, G. Courtine, J. Guck, *Nat. Rev. Mater.* **2016**, *1*, 16063.
[9] R. Portillo-Lara, J. A. Goding, R. A. Green, *Curr. Opin. Biotechnol.* **2021**, *72*, 62.

[10] Y. D. P. Limasale, P. Atallah, C. Werner, U. Freudenberg, R. Zimmermann, *Adv. Funct. Mater.* **2020**, *30*, 2000068.
[11] R. Zimmermann, C. Hentschel, F. Schrön, D. Moedder, T. Büttner, P. Atallah, T. Wegener, T. Gehring, S. Howitz, U. Freudenberg, C. Werner, *Biofabrication* **2019**, *11*, 045008.
[12] T. S. Wilems, X. Lu, Y. E. Kurosu, Z. Khan, H. J. Lim, L. A. S. Callahan, *J. Biomed. Mater. Res., Part A* **2017**, *105*, 3059.
[13] C. Tondera, T. F. Akbar, A. K. Thomas, W. Lin, C. Werner, V. Busskamp, Y. Zhang, I. R. Minev, *Small* **2019**, *15*, 1901406.
[14] R. Fernandes, L.-Q. Wu, T. Chen, H. Yi, G. W. Rubloff, R. Ghodssi, W. E. Bentley, G. F. Payne, *Langmuir* **2003**, *19*, 4058.
[15] R. A. Zangmeister, J. J. Park, G. W. Rubloff, M. J. Tarlov, *Electrochim. Acta* **2006**, *51*, 5324.
[16] M. Cheong, I. Zhitomirsky, *Colloids Surf., A* **2008**, *328*, 73.
[17] X. W. Shi, C.-Y. Tsao, X. Yang, Y. Liu, P. Dykstra, G. W. Rubloff, R. Ghodssi, W. E. Bentley, G. F. Payne, *Adv. Funct. Mater.* **2009**, *19*, 2074.
[18] X. Cheng, U. A. Gurkan, C. J. Dehen, M. P. Tate, H. W. Hillhouse, G. J. Simpson, O. Akkus, *Biomaterials* **2008**, *29*, 3278.
[19] M. Lei, X. Qu, H. Wan, D. Jin, S. Wang, Z. Zhao, M. Yin, G. F. Payne, C. Liu, *Sci. Adv.* **2022**, *8*, eabl7506.
[20] E. Servoli, D. Maniglio, A. Motta, C. Migliaresi, *Macromol. Biosci.* **2008**, *8*, 827.
[21] Y. Lin, X. Xia, K. Shang, R. Elia, W. Huang, P. Cebe, G. Leisk, F. Omenetto, D. L. Kaplan, *Biomacromolecules* **2013**, *14*, 2629.
[22] J. Li, E. Kim, K. M. Gray, C. Conrad, C.-Y. Tsao, S. P. Wang, G. Zong, G. Scarcelli, K. M. Stroka, L.-X. Wang, W. E. Bentley, G. F. Payne, *Adv. Funct. Mater.* **2020**, *30*, 2001776.
[23] U. Freudenberg, P. Atallah, Y. D. P. Limasale, C. Werner, *Faraday Discuss.* **2019**, *219*, 244.
[24] Z. Fei, B. Liu, M. Zhu, W. Wang, D. Yu, *Cellulose* **2018**, *25*, 3179.
[25] K. Jin, E. K. Leitsch, X. Chen, W. H. Heath, J. M. Torkelson, *Macromolecules* **2018**, *51*, 3620.
[26] Y. Ma, Z. Guo, X. Dong, Y. Wang, Y. Xia, *Angew. Chem., Int. Ed.* **2019**, *58*, 4622.
[27] D. T. Bacheschi, E. Z. Strittmatter, S. Sawtelle, M. Nami, *Micromachines* **2022**, *13*, 141.
[28] J. Lee, J. W. Mullen, G. Hussain, D. S. Silvester, *Electrochim. Acta* **2021**, *384*, 138412.
[29] B. Fan, B. Wolfrum, J. T. Robinson, *J. Neural Eng.* **2021**, *18*, 056025.
[30] Q. Zhang, D. Ren, S. Pan, M. Wang, J. Luo, Y. Zhao, M. Grätzel, X. Zhang, *Adv. Funct. Mater.* **2021**, *31*, 2103966.
[31] C. Bodart, N. Rossetti, J.'E. Hagler, P. Chevreau, D. Chhin, F. Soavi, S. B. Schougaard, F. Amzica, F. Cicoira, *ACS Appl. Mater. Interfaces* **2019**, *11*, 17226.
[32] C. F. Lourenço, M. Caetano, A. Ledo, R. M. Barbosa, *Bioelectrochemistry* **2019**, *130*, 107325.
[33] W. Tao, D. Pan, Z. Gong, X. Peng, *Anal. Chim. Acta* **2018**, *1035*, 44.
[34] L. Liu, S. Yellinek, I. Valdinger, A. Donval, D. Mandler, *Electrochim. Acta* **2015**, *176*, 1374.
[35] Y. Wang, Y. Liu, Y. Cheng, E. Kim, G. W. Rubloff, W. E. Bentley, G. F. Payne, *Adv. Mater.* **2011**, *23*, 5817.
[36] J. Hu, M. F. Yu, *Science* **2010**, *329*, 313.
[37] K. Mckelvey, M. A. O'connell, P. R. Unwin, *Chem. Commun.* **2013**, *49*, 2986.
[38] K. Yan, C. Yang, W. Zhong, Z. Lu, X. Li, X. Shi, D. Wang, *Soft Matter* **2020**, *16*, 9471.
[39] L. W. Lau, R. Cua, M. B. Keough, S. Haylock-Jacobs, V. W. Yong, *Nat. Rev. Neurosci.* **2013**, *14*, 722.
[40] C. E. Hoyle, C. N. Bowman, *Angew. Chem., Int. Ed.* **2010**, *49*, 1540.
[41] J. Nie, J. P. Li, H. Deng, H. C. Pan, *Chinese J. Anal. Chem.* **2015**, *43*, 609.
[42] O. Norberg, I. H. Lee, T. Aastrup, M. Yan, O. Ramström, *Biosens. Bioelectron.* **2012**, *34*, 51.
[43] S. Yigit, R. Sanyal, A. Sanyal, *Chem. - Asian J.* **2011**, *6*, 2648.
[44] S. Ciampi, T. Böcking, K. A. Kilian, J. B. Harper, J. J. Gooding, *Langmuir* **2008**, *24*, 5888.
[45] P. J. Brewer, R. J. Leese, R. J. C. Brown, *Electrochim. Acta* **2012**, *71*, 252.
[46] A. M. Hussain, J. V. T. Høgh, W. Zhang, P. Blennow, N. Bonanos, B. A. Boukamp, *Electrochim. Acta* **2013**, *113*, 635.

